AIAA JOURNAL
Vol. 38, No. 3, March 2000

Application of Neural Networks to Stereoscopic Imaging Velocimetry

Yi Ge* and Soyoung Stephen Cha†
University of Illinois at Chicago, Chicago, Illinois 60607-7022

Stereoscopic imaging velocimetry is an optical nonintrusive method for measuring three-dimensional three-component gross-field fluid flows that is based on the images captured by two charge-coupled device sensors from different vantage points. In this approach part of the individual particle images or equivalent data points are likely to be lost when a flowfield with a high-particle density is captured by the imaging system. The data loss and erroneous detection mostly occur during the process of overlap decomposition of superimposed particle images and during the phase of particle tracking. To maximize the data point recovery and to enhance the measurement reliability by correctly identifying particles and tracks, neural networks are implemented in the two phases of stereoscopic imaging velocimetry. For the phase of particle overlap decomposition, the back propagation neural network is used because of its ability in pattern recognition and nonlinear classification. For the phase of particle tracking, the Hopfield neural network is employed to attain a globally optimal solution in finding appropriate particle tracks. Our investigation indicates that the neural networks offer very good potential for performance enhancement and has proven to be very useful for stereoscopic imaging velocimetry.

Introduction

TO understand accurately various aspects of complex fluid flows, either steady or transient, which arise in many modern engineering applications, it is very necessary to develop the measurement techniques capable of providing three-dimensional, three-component (3-C) velocity information. Currently, several approaches and corresponding algorithms have been available for two-dimensional velocimetry based on the images captured by a single camera, that is, particle-imaging velocimetry (PIV). For velocity extraction in PIV, cross correlation can be one of the mostly known algorithms.[1] It yields two-dimensional velocity information without ambiguity in flow direction over a plane from separately exposed images of flow tracer particles.

Traditionally, the approaches for three-dimensional, 3-C velocimetry are based on stereoscopic or holographic image observation.[2–6] Recently, the development of stereoscopic-imaging velocimetry (SIV) has been reported by some investigators.[3,4] The SIV is advantageous in system simplicity for building compact hardware and in software efficiency for continual near-real-time velocity monitoring. It, however, has a limitation in observing an extended area with high resolution. In our configuration the SIV system consists of two charge-coupled device (CCD) cameras, oriented relatively at a 90-deg angle with respect to each other in observing a fluid experiment. The data processing of the images captured by the SIV system is composed of the following steps in sequence: camera calibration, particle centroid determination and overlap decomposition, particle tracking, stereo-matching, and velocity vector validation.

In the SIV processing the data points are usually lost in the processes of overlap decomposition of superimposed particle images and particle tracking. In an effort to alleviate the problem of data loss during these two phases of processing, we have implemented the artificial neural networks to the SIV system. Artificial neural networks are parallel computational models that comprise densely interconnected adaptive processing units. A very important feature of these networks is their adaptive nature, where learning by example replaces programming in solving problems.[7,8] Because of its ability in pattern recognition and nonlinear classification, the back propagation (BP) neural network is utilized for the phase of particle overlap decomposition. The Hopfield neural network is adopted to attain globally optimal solutions in the phase of particle tracking. Although the use of neural networks is computationally intensive in training stages, decomposition of particle blobs and attainment of optimal particle tracks can be made very efficient with modern computational hardware and software. Briefly, it is believed that the application of neural networks to SIV can provide appropriate means for enhancing three-dimensional flow diagnostics of a restricted volume in real time with reasonable measurement accuracy.

Description of Method

BP Neural Network for Particle Overlap Decomposition

For particle overlap decomposition the BP neural network has been employed owing to nonlinear classifying ability. Back propagation is a supervised learning method in which an error signal is fed back through the network by altering weights to prevent the same error from repeating in the process. The network is trained by presenting it with input and output pairs of known answer. The weights are changed so that the network eventually produces the matching output pattern when given the corresponding input pattern of the pair. In designing the BP neural network for decomposing overlapping particle image blobs, three layers are chosen. They are the input, hidden, and output layer, respectively, as shown in Fig. 1. The transfer (activation) function that is used by each neuron is the sigmoid function. If x is the summed input of a neuron, the output of the neuron is given by Eq. (1):

$$f(x) = (1/1 + e^{-x}) \tag{1}$$

Let P denote the number of the total learning samples; x^1, $x^2, \ldots, x^P$ denote the input of the learning samples; $t^1, t^2, \ldots, t^P$ are the target output of the learning samples; and $y^1, y^2, \ldots, y^P$ are the actual output of the neural network. Let y_k be the kth output of the output layer (responses of the network); z_j is the jth output of the hidden layer, and x_i is the ith output of the input layer. From Fig. 1,

$$y_k = f\left(\sum_{j=1}^{J} w_{jk} z_j\right) \tag{2}$$

$$z_j = f\left(\sum_{i=1}^{I} w_{ij} x_i\right) \tag{3}$$

Presented as Paper 98-2812 at the AIAA 29th Fluid Dynamics Conference, Albuquerque, NM, 15–18 June 1998; received 4 December 1998; revision received 12 August 1999; accepted for publication 17 August 1999.

*Graduate Assistant, M/C 251, Department of Mechanical Engineering, 842 West Taylor Street.
†Associate Professor, M/C 251, Department of Mechanical Engineering, 842 West Taylor Street. Senior Member AIAA.

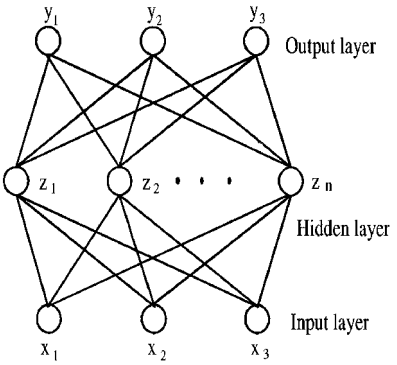

Fig. 1 BP neural network.

where w_{jk} are the weights (connection strengths) between the hidden layer and the output layer and w_{ij} are the weights between the input layer and the hidden layer. J is the number of neurons in the hidden layer, and I is the number of neurons in the input layer. For P learning samples the total error can be calculated as

$$E_{\text{total}} = \frac{1}{2}\sum_{p=1}^{P}\sum_{k=1}^{K}\left(t_k^p - y_k^p\right)^2 \tag{4}$$

where K is the number of neurons in the output layer.

In training, the network involves an iterative procedure in which the samples are sequentially presented repeatedly to the network. To minimize the error at each time of iteration, which is the difference between the target output and the actual output of the network, the weights between each layer must be altered. The network propagates the error backward, altering the weights from the output layer to the input layer.

Based on Eq. (4), the iteration formula of the weight changes between each layer can be obtained by

$$\Delta w_{jk} = -\eta\frac{\partial E_{\text{total}}}{\partial w_{jk}} \tag{5}$$

$$\Delta w_{ij} = -\eta\frac{\partial E_{\text{total}}}{\partial w_{ij}} \tag{6}$$

where η is the step size or the learning rate of the network. By applying the chain rule in calculus,

$$\frac{\partial E_{\text{total}}}{\partial w_{jk}} = -\sum_{p=1}^{P}\delta_{jk}^p z_j^p \tag{7}$$

where $\delta_{jk}^p = (t_k^p - y_k^p)y_k^p(1 - y_k^p)$ and

$$\frac{\partial E_{\text{total}}}{\partial w_{ij}} = -\sum_{p=1}^{P}\delta_{ij}^p x_i^p \tag{8}$$

where

$$\delta_{ij}^p = \sum_{k=1}^{K}\delta_{jk}^p w_{jk} z_j^p\left(1 - z_j^p\right)$$

Equations (7) and (8) can be used in the iterative process for altering the weights between each layer until the error is minimized to a satisfactory level.

Our initial study showed that overlapping particles could be resolved by human eyes based on the two features of circumference and major axis length of an image element. We consider that the pixel area of an individual particle image is also very important. We thus used these three features of particles as the input to the network. That is, the important feature parameters for distinguishing the overlapping particles are area, circumference, and major-axis length. The target output is the probability that indicates an image element to be a single particle image and an overlapping image of double or triple particles. For training, the weights were initially assigned arbitrarily. Then the three features of particle images were provided as the input to the network along with the target output. The network runs forward from the input layer to the output layer, providing the actual responses of the network to the given inputs. Errors are calculated by comparing the actual responses of the network with the given targets. The iterative procedure then traces back from the output layer to the input layer, changing the weights between the output layer and hidden layer and between the hidden layer and input layer. After the errors are reduced to an appropriate range, the iteration is terminated, and the network is used to identify image elements.

Hopfield Neural Network for Particle Tracking

Particle tracking is a phase in our SIV system where particle images in consecutive frames, which are captured by a CCD camera, are identified as those for the same particle. For extracting a velocity map at a moment, four sequential frames are selected from the continuous frames and analyzed as a batch. By performing the steps of particle overlap decomposition and centroid determination, individual particles are identified in the first frame, that is, frame 1 of the track sequence. Candidate particles are then identified in frame 2 by searching them in a circle based on the maximum estimate of flow velocity. In the next step candidate particles in frame 3 are identified using position estimation for each of the possible tracks obtained from frames 1 and 2. This process is repeated for the fourth frame.

Additionally, the fourth frame can be used to provide a check on the validity of an assumption of smooth track velocity. After all possible tracks are found through four time-sequential frames, the Hopfield neural network is used to select an ideal track from the database of potentially valid tracks. To get a high successful recovery rate, the following requirements for global optimization need be imposed: 1) an ideal track should be smooth, i.e., the local velocity and acceleration should be consistent; 2) a particle can belong only to a single track; and 3) the optimal tracking can maximize the number of completed tracks.

The Hopfield neural network is composed of a single layer of neurons. The neurons are symmetrically connected (i.e., $w_{ij} = w_{ji}$). Every neuron is connected to all other neuron. Each neuron is nonlinear and can assume output from 0 to 1. At each point in time, the state of a neuron is characterized by the activation dynamics given by

$$C_i\frac{\mathrm{d}x_i}{\mathrm{d}t} = \sum_{j=1}^{M} w_{ij}v_j + I_i - \frac{x_i}{R_i}, \qquad i = 1, 2, \ldots, M$$

$$v_i = F(x_i) \tag{9}$$

where w_{ij} is the connection weight from neuron i to neuron j, x_i is the activation of the ith neuron, and v_j is the output of jth neuron. M is the total number of neurons in the network that is used to represent the number of possible tracks, and I_i is the external input to neuron i. $F(x)$ is the sigmoid function. C_i and R_i are constants. The stable states of a network with dynamics given by Eq. (9) are the minima of the energy function

$$E = -\frac{1}{2}\sum_{i=1}^{M}\sum_{j=1}^{M} w_{ij}v_i v_j - \sum_{i=1}^{M} v_i I_i + \sum_{i=1}^{M}\frac{1}{R_i}\int_0^{v_i} F^{-1}(\eta)\,\mathrm{d}\eta \tag{10}$$

provided that $w_{ij} = w_{ji}$ for all $i \neq j$ and $w_{ii} = 0$ for all i.

By considering three requirements in the optimization scheme just mentioned, the energy function can be expressed in an appropriate form of

$$E = A\sum_{i=1}^{M}(v_i \times \text{Error}_i) + B\sum_{i=1}^{M} v_i(v_{i1} + v_{i2} + \cdots + v_{\text{in}}) + C\left(\sum_{i=1}^{M} v_i - N\right)^2 \tag{11}$$

where A, B, and C are constants. N is the number of proper tracks, and n is the number of other tracks that the same particle image points coincide with the ith track; $v_{i1}, v_{i2}, \ldots, v_{\text{in}}$ are tracks that compete the same particle image points with ith track. In the energy function given by Eq. (11), the first term on the right-hand side is used to account for the smoothness of particle tracks. The second term is used to account for the requirement that one particle should

belong to one track only. The last term is used to meet the requirement that the number of completed tracks should be maximized. The term Error_i that is employed to evaluate the smoothness of a track can be expressed as follows:

$$\begin{aligned}\text{Error}_i = &\left[(V_{1x} - \bar{V}_x)^2 + (V_{1y} - \bar{V}_y)^2 + (V_{2x} - \bar{V}_x)^2\right. \\ &+ (V_{2y} - \bar{V}_y)^2 + (V_{3x} - \bar{V}_x)^2 + \left.(V_{3y} - \bar{V}_y)^2\right] \\ &+ \left[(a_{2x} - a_{1x})^2 + (a_{2y} - a_{1y})^2\right] \end{aligned} \tag{12}$$

with

$$\begin{aligned} \bar{V}_x &= (V_{1x} + V_{2x} + V_{3x})/3, & \bar{V}_y &= (V_{1y} + V_{2y} + V_{3y})/3 \\ a_{1x} &= (V_{2x} - V_{1x})/\,\mathrm{d}t, & a_{2x} &= (V_{3x} - V_{2x})/\,\mathrm{d}t \\ a_{1y} &= (V_{2y} - V_{1y})/\,\mathrm{d}t, & a_{2y} &= (V_{3y} - V_{2y})/\,\mathrm{d}t \end{aligned} \tag{13}$$

where $\bar{V}_x$ and $\bar{V}_y$ are the average velocity in the x and y directions of each track appearing in four two-dimensional time-sequence image frames; (V_{ix}, V_{iy}) are local velocities of a track extracted for the ith frame calculated with particle's positions in the $(i + 1)$th frames; (a_{ix}, a_{iy}) are the x and y components of the local acceleration for the ith frame calculated with the particle positions in the following two frames; and $\mathrm{d}t$ is the time interval between two frames. By these definitions a good track should have a smaller Error_i value.

The network may take a number of iterations to be able to arrive at a stable state. To make the energy function minimized along with the iterations, the following requirement should be met:

$$\begin{aligned}\frac{\mathrm{d}x_i}{\mathrm{d}t} &= -\frac{\partial E}{\partial v_i} \\ &= -A\text{Error}_i - 2B(v_{i1} + v_{i2} + \cdots + v_{\text{in}}) - 2C\left(\sum_{i=1}^{M} v_i - N\right)\end{aligned} \tag{14}$$

By comparing Eqs. (9) and (13), we get

$$w_{ij} = \begin{cases} -2C & \text{if} \quad v_j \notin [v_{i1}, v_{i2}, \ldots, v_{\text{in}}] \\ -(2B + 2C) & \text{if} \quad v_j \in [v_{i1}, v_{i2}, \ldots, v_{\text{in}}] \end{cases}$$

$$I_i = -A \cdot \text{Error}_i + 2CN \tag{15}$$

With all of these definitions, the Hopfield neural network to be used for particle tracking is complete for construction.

If we plot the energy function, a three-dimensional curved surface can be generated. The areas of minimum energy, that is, the stable states or energy minima, appear as valleys. Each of these local minima can end up as one possible solution.

Experimental Results

To implement the concept of the BP neural network for particle overlap decomposition and to evaluate its performance, 600 image elements (blobs) were experimentally collected for various values of particle size, distance to the imaging system, lighting condition, etc. In the BP neural network processing, binarized particles images are employed for extraction of feature parameters. Figure 2 shows these binarized real particle images collected with an imaging system and a CCD camera. These either overlapping or nonoverlapping particle images consisted of one, two, and three particles. In imaging the average image size of single particles was around 3–5 pixels in diameter. The 600 particle images were divided into two sets of equal number in images. The first set was used to train the BP neural network. As indicated, the three major features of image elements, that is, area, circumference, and major-axis length were provided as the input to the network. After the network minimized the error and correctly obtained most of the output through an iterative process, the network was tested by using the second set.

Through the testing with the BP neural network, the percentage of successful classification and decomposition of particle images was obtained. The analysis was performed for two trials. For the second trial, the second set was for training of the network, whereas the first one was for testing. Table 1 shows the percentage of successful identification and decomposition of the particle blobs in both of the trials and the average percentage of successful identification. The results demonstrate a successful performance of the neural network in particle overlap decomposition.

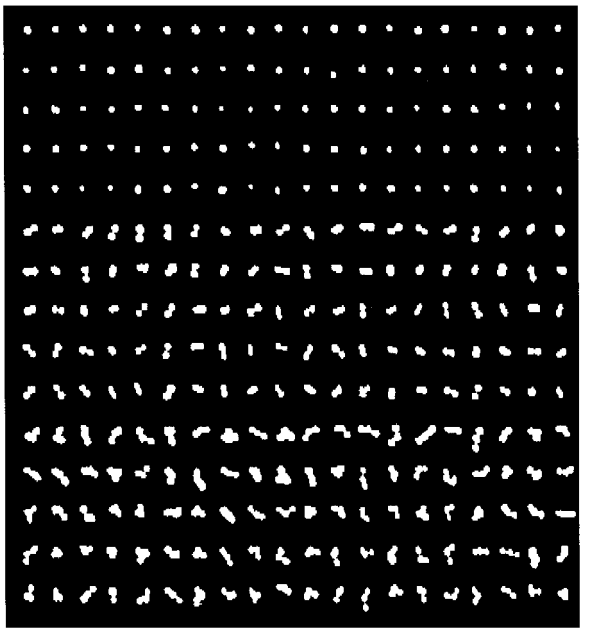

a) Data set 1

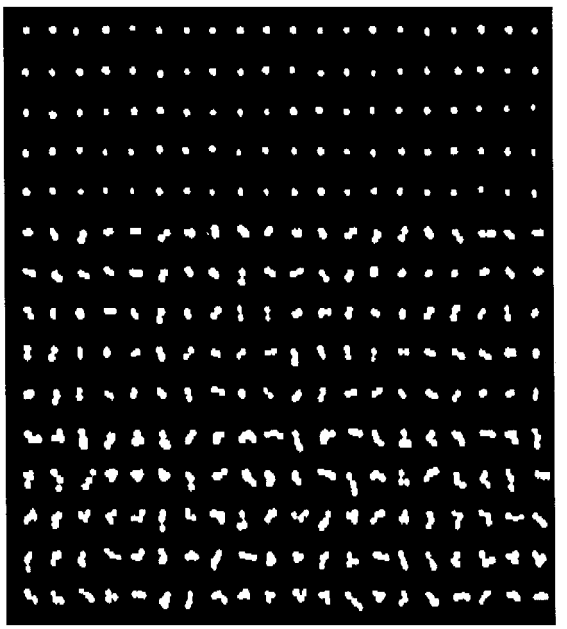

b) Data set 2

Fig. 2 Data sets of real particle images captured by CCD cameras after binarization.

To investigate and test the use of the neural networks for SIV with more realistic flowfields, water seeded with 100-μm polystyrene particles was ejected from a sharp tube tip into a 280 × 280 × 280 mm test section filled with water. As seen in Fig. 3, a slightly protruding tube of 760-mm length and 12.7-mm inner diameter was located vertically at the bottom of the test section. Our system simulated a free jet flow with as parabolic velocity profile at the tube tip. Two Sony XC-8500CE noninterlace CCD cameras of 782 × 582 pixels were positioned orthogonally at an equal distance of 267 mm from the tube center, which could capture images at a rate of 25 frames per second. At this configuration both cameras could capture the jet flow seeded with particles emerging from the tube tip region of 12.7 × 12.7 × 12.7 mm, which corresponds to the processed area of 512 × 512 pixels in image projection.

Table 1 Percentage of successful identification and decomposition of overlapping particle images by using the BP neural network

Trial	Training set	Testing set	% 1 particle	% 2 particles	% 3 particles
1	1	2	100	89	93
2	2	1	96	85	90
Average percentage of successful identification			98	87	91.5

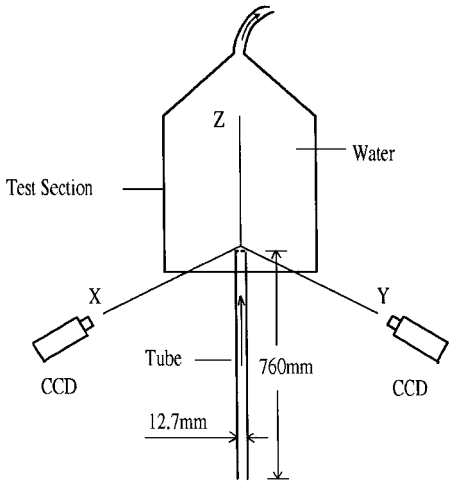

Fig. 3 Schematic of the experimental setup.

By using the tested BP neural network in particle decomposition and the Hopfield neural network in particle tracking, the velocity of the jet flow near the tip of the tube was measured. The particle centroid could be identified with accuracy better than one-tenth of a pixel. The maximum particle displacement between two consecutive image frames was about 20 particle diameters. With the measured mean velocity V of 25 mm/s within the vertical tube of diameter D and the viscosity μ of water at the room temperature, the Reynolds number Re was about 300. The tube length ℓ was sufficiently long such that $\ell/D > 0.06Re$. A fully developed parabolic laminar velocity profile was thus expected, starting from the tube exit. However, it was confined only to the core region where the fluid was undisturbed by the freejet boundary. Figures 4a and 4b are typical particle images of the test flow captured by both of the cameras at a moment. There were more than 300 particles captured in each frame. Figure 5 shows the two-dimensional velocity fields extracted from the images of each camera as shown in Fig. 4. Figure 6 shows the three-dimensional velocity field of the flow after stereo-matching of the two-dimensional velocity information from each camera. There were incomplete or invalid tracks across the four two-dimensional frames primarily owing to the particles going in and out of the measured volume, from which particle tracks are extracted. This resulted in three-dimensional data points about 15% less than the number of particles appearing in stereo matching. For demonstration the flow velocity in the z direction is plotted in Fig. 7 for the x–y cross section at the tube exit. The limited data points right at the tube tip, that is, number of particles, and the artifact of the plotting software did not allow a smooth plot near the center. However, in general, the parabolic behavior of the velocity profile can be observed in the plot. As expected, the particle velocities had the maximum value along the pipe centerline and decreased outward to become a fluctuating boundary flow.

To assess the accuracy of the developed system, the experimental results were compared with the laminar velocity profile $u(r)$ at a radial position r in a circular pipe, which can be described by formula $u(r) = 2U_{\text{avg}}[1 - (r/R)^2]$. Here U_{avg} and R are average velocity and pipe radius, respectively. The results after the final velocity validation process, for screening out those erroneous tracks that differ too much from their neighbors, are shown in Fig. 8. The average of the difference between the measured values and the

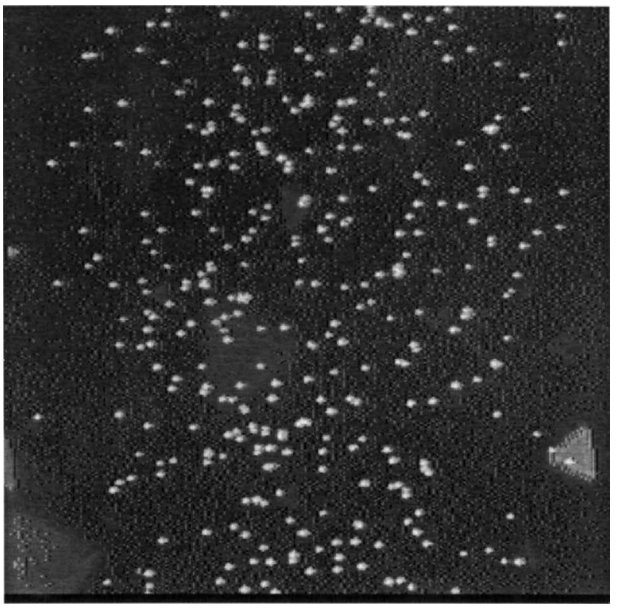

a) Left camera

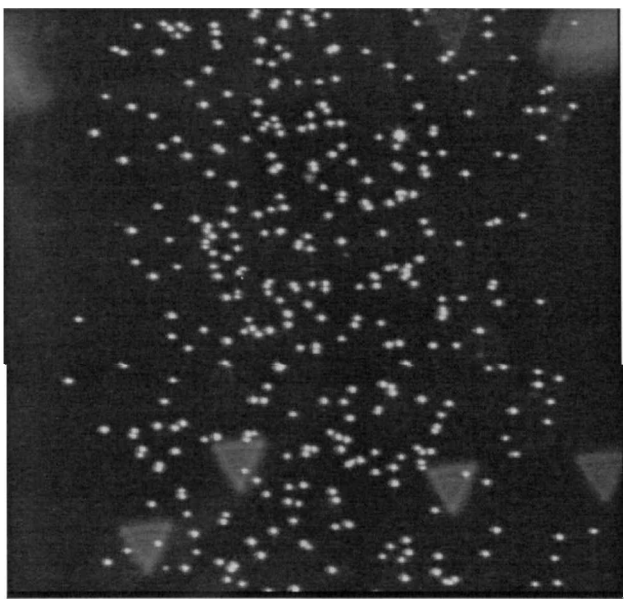

b) Right camera

Fig. 4 Particle images of the freejet flow captured by cameras.

parabolic velocity profile was about 8.9% of the maximum velocity. As expected, the difference mostly occurred near the freejet boundary, where the experimental results are slightly lower than the initial parabolic velocity profile. It is believed that this is because the laminar flow emerging from the tube tip is affected by the viscous ambient fluid to gradually become turbulent. At the core region with a radius less than 1mm, where the flow is believed to be unaffected by the jet boundary, the deviation was less than 0.83% of the maximum value. For the core region with a radius less than 2 mm, the deviation was 3.1%. It can thus be reasonable to conservatively

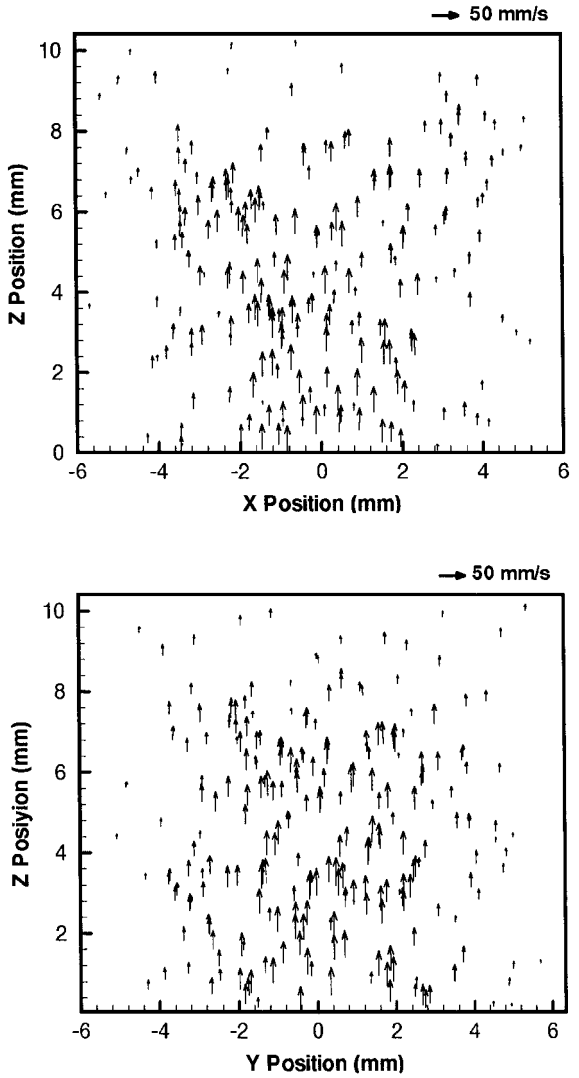

Fig. 5 Two-dimensional velocity field extracted from the images of each camera.

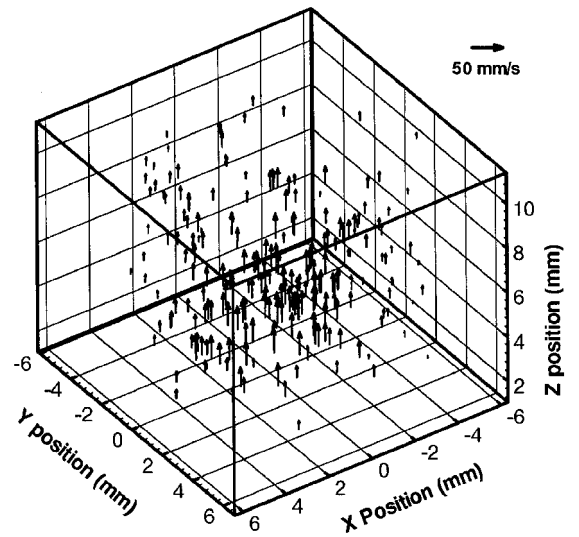

Fig. 6 Three-dimensional velocity field obtained with two cameras.

estimate the measurement accuracy better than 3.1%. It is believed that the data recovery rate and measurement accuracy deteriorate as particle density increases because of difficulties in accurately identifying particle centroids and particle tracks. These can further be enhanced in the future through improvement of the current neural network approaches, hybridization of conventional processing techniques including cross correlation of images, and application of rigorous velocity validation processes based on flow physics.

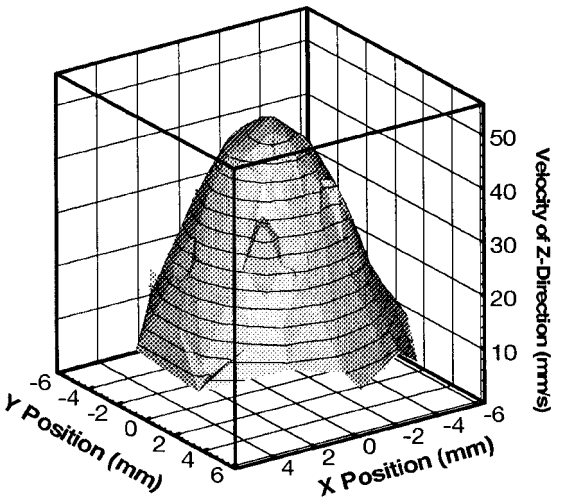

Fig. 7 Velocity profile at the nozzle tip obtained by the SIV system.

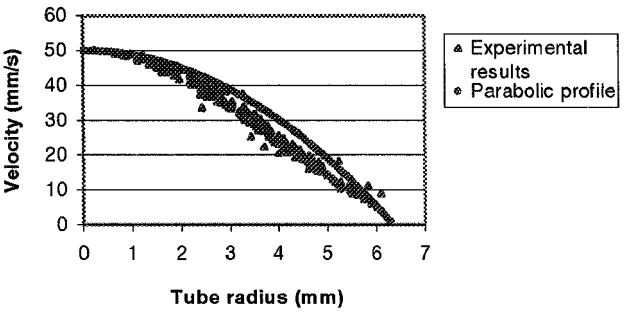

Fig. 8 Measured velocities and the plot of the parabolic profile.

Conclusion

Owing to the efficiency in pattern recognition and nonlinear classification, the BP neural network has been employed in identification and decomposition of overlapping particle images in a SIV system. The results have shown that on the average more than 92% of real image elements, with equal weights in population for singly, doubly, and triply superimposed particle images, can be successfully identified and decomposed if necessary by using the BP neural network. In actual experiments the population of single particles far exceeds those of multiply overlapping particles and the success rate can be much greater. The utilization of the Hopfield neural network has proven to be very useful in attaining potentially valid particle tracks whose track assignments correspond to a desired global-optimization scheme. Based on our experiments for a realistic flowfield, the results have demonstrated significant advantages in using the neural networks, with a good agreement between the experimental and theoretical velocity profiles.

Although the implementation of the neural networks to the SIV system is in a developmental stage, the initial experimental results have shown it to be a promising method for accurate three-dimensional, 3-C velocity extraction in real time. Future investigations will focus on further improving processing efficiency and measurement performance for practical applications including the use of small particles. It is believed that the use of artificial neural networks in the SIV system can become an important approach with the ability to meet the increasing demands of the modern fluid flow research especially for microgravity experiments.

Acknowledgment

This work is supported by NASA Grant Nag 8-1248.

References

[1]Cha, S. S., Slepicka, J. S., Sun, H., and Cho, Y. C., "Application of Digital Image Velocimetry to Displacement Measurements," *Proceedings of Hologram Interferometry and Speckle Metrology*, Society for Experimental Mechanics, Bethel, CT, 1990, pp. 81–87.

[2]Slepicka, J. S., and Cha, S. S., "Holographic Diffraction Image Velocimetry for Measurement of Three-Dimensional Velocity Fields," *AIAA Journal*, Vol. 35, No. 7, 1997, pp. 1201–1203.

[3]Guezennec, Y. G., Brodrey, R. S., and Kent, J. C., "Algorithm for Fully Automated Three-Dimensional Particle Tracking Velocimetry," *Experiments in Fluids*, Vol. 17, No. 4, 1994, pp. 209–219.

[4]Meyer, M. B., Bethea, M. D., Guezennec, Y. G., and Choi, W. C., "Stereo Imaging Velocimetry: A New Option for Microgravity Experiments," *Proceedings on Fluid Mechanics Phenomena in Microgravity*, AMD-Vol.174/FED-Vol.175, American Society of Mechanical Engineers, New York, 1993, pp. 173–182.

[5]Elkins, R. E., Jackman, G. R., and Johnson, R. R., "Evaluation of Stereoscopic Trace Particle Records of Turbulent Flow Fields," *Review of Scientific Instruments*, Vol. 48, No. 7, 1977, pp. 738–746.

[6]Adamczyk, A. A., and Rimai, L., "Reconstruction of Three-Dimensional Flow Field from Orthogonal View of Seed Track Video Images," *Experiments in Fluids*, Vol. 6, No. 6, 1988, pp. 380–386.

[7]Rumelhart, D. E., Hinton, G. E., and Williams, R. J., *Parallel Distributed Processing: Explorations in the Microstructure of Cognition*, MIT Press, Cambridge, MA, 1986, pp. 318–362.

[8]Ripley, B. D., *Pattern Recognition and Neural Networks*, Cambridge Univ. Press, Cambridge, England, U.K., 1996.

R. P. Lucht
Associate Editor